Nanomedicine: Nanotechnology, Biology, and Medicine
17 (2019) 254–265

nanomedicine
Nanotechnology, Biology, and Medicine

nanomedjournal.com

# HBO1 directs histone H4 specific acetylation, potentiating mechano-transduction pathways and membrane elasticity in ovarian cancer cells

Marcos Quintela, PhD[a,b], Douglas H. Sieglaff, PhD[b], Andrea Salvatore Gazze, PhD[a], Aijun Zhang, MD[b], Deyarina Gonzalez, PhD[a], Lewis Francis, PhD[a], Paul Webb, PhD[b], R. Steven Conlan, PhD[a,*]

[a]*Swansea University Medical School, Swansea, Wales, United Kingdom*
[b]*Houston Methodist Research Institute, Houston, TX, United States*

Revised 25 January 2019

**Abstract**

New approaches to treat ovarian cancer, the fifth leading cause of cancer mortality among women, are being sought, with the targeting of epigenetic modulators now receiving much attention. The histone acetyltransferase HBO1 functions in regulating diverse molecular processes, including DNA repair, transcription and replication, and is highly expressed in primary ovarian cancer. Here we define both the molecular function and a role in cell biomechanics for HBO1 in ovarian cancer. HBO1 preferentially acetylates histone H4 through the concomitant overexpression of co-regulator JADE2, and is required for the expression of YAP1, an ovarian cancer oncogene and mechano-transductor signaling factor. HBO1 appears therefore to have a role in determining the mechano-phenotype in ovarian cancer cells, through both signal transduction processes, and the modulation of cell elasticity as observed using direct measurements on live cells via atomic force microscopy.


*Key words:* Acetyltransferase; JADE; YAP1; Elasticity; Biomechanics

Alterations in epigenetic regulatory mechanisms play important roles in tumorigenesis and changes in histone acetylation/deacetylation have been implicated in a variety of cancers.[1] Histone acetyltransferase (HAT) binding to ORC-1 (HBO1, also known as KAT7 and MYST2) is a member of the MYST family of HATs,[2] nuclear proteins that function within large multicomponent protein complexes. The HBO1-complex is recruited by tri-methylated histone H3 at lysine (K) 4 and 36, is responsible for H4 acetylation at K5, 8, 12 and 16[3,4] and also mediates H3 acetylation at K14.[5,6] HBO1 is enriched near transcriptional start sites and within gene coding regions,[6,7] acts as a specific co-activator for steroid receptors (estrogen receptor alpha, progesterone receptor) and other transcription factors[8–10] and represses activities of others, including NF-κβ, probably via co-activator sequestration.[11,12] Other components of the HBO1-complex include the inhibitor of growth (ING) tumor suppressor proteins 4/5, the Esa-associated factor 6 (Eaf6) and scaffolding subunits (JADE1/2/3 and BRPF1/2/3),[3,6,7] the latter being responsible for directing HBO1-complexes to distinct chromatin regions, defining substrate specificity.[13,14]

Several lines of evidence suggest that HBO1 is important in cancers, and it has been found overexpressed in ovarian carcinoma, breast adenocarcinoma and testicular germ cell tumors.[4] Further,

*Abbreviations:* OC, ovarian cancer; HAT, histone acetyltransferase; ING, inhibitor of growth; KD, knockdown; HGSC, high-grade serous carcinoma; AFM, atomic force microscopy; HOSEpiC, human ovarian surface epithelial cells

Funding: This work was supported by the Natural and Environmental Research Council (NERC), UK [grant number NE/K004212/1]; Houston Methodist Research Institute; and Swansea University.

Conflict of interest: The authors declare no conflict of interest

*Corresponding author at: Swansea University Medical School, Swansea University, Singleton Park, Swansea, SA2 8PP, United Kingdom.
*E-mail address:* r.s.conlan@swansea.ac.uk. (R.S. Conlan).

https://doi.org/10.1016/j.nano.2019.01.017

the *HBO1* locus (17q21.3) maps to a region that shows frequent allelic gains associated with poor prognosis in breast cancers.[15,16] Transient knockdown (KD) of HBO1 potentiates anti-estrogen-dependent growth suppression of MCF-7 cells[17] and reduces proliferation in several non-breast cell types such as 293 T[3] and MLE-12 cells.[18] While these findings collectively point to cancer promoting and pro-proliferative activities, HBO1 can also play anti-oncogenic roles in other cell types; HBO1 expression is suppressed in acute myeloid leukemia and its depletion increases colony formation of THP-1 and SEM leukemic cell lines.[19] Further, *HBO1−/−* mice are non-viable with specific post-gastrulation defects, but cells from pre-gastrulation *HBO1−/−* mice proliferate normally.[5] Instead, *HBO1−/−* embryos display reduced expression of genes required for embryonic patterning along with reduced acetylated H3K14, with no effects on H4 acetylation. Thus, HBO1 is not always required for cell division and influences behavior of different cell types in distinct ways.

Ovarian cancer (OC) is one of the five leading causes of female cancer mortality worldwide and survival rates have improved little in the last 30 years.[20,21] Mortality is due to the asymptomatic nature of early disease and lack of long-term effective treatment strategies for advanced conditions. There are five distinct major ovarian cancer histo-types (high-grade/low-grade serous, endometrioid, clear-cell and mucinous), which exhibit distinct clinical features, responses to chemotherapy and outcomes.[22] Within these categories, high-grade serous carcinoma (HGSC) has the worst prognosis and the highest mortality rates and represents ~70% of epithelial ovarian cancer.[22] HGSC almost always contains mutated *TP53* (~95%) and about 20% of tumors contain germline or somatic mutations in breast cancer susceptibility genes (*BRCA1/2*). Other features are defects in homologous recombination DNA repair pathways (50%), *CCNE1* amplification and broad genomic instability.[23–25]

Since HBO1 is overexpressed in OC and is frequently associated with enhanced cell division,[4] we set out to elucidate its functions in OC cells. Reduction of HBO1 expression by synthetic knockdown of HBO1 identified a specific role in the acetylation of histone H4, and not H3K14 acetylation. Gene expression analysis determined that the mechano-transductor signaling factor YAP1 was regulated by HBO1, supporting bioinformatic analysis which suggested that cell viability, motility and cytoskeletal reorganization pathways were altered following manipulation of HBO1 expression. This prediction was confirmed through analysis of the biomechanical properties of OC cells using atomic force microscopy (AFM). The overexpression of HBO1 in OC cells resulted in elevated cell elasticity as determined by significantly lower Young's modulus compared to cells subjected to synthetic HBO1 knockdown, and reveals a link between epigenetic processes and cell mechanical properties associated with aggressive OC phenotypes.

## Methods

### *Cell culture*

The ovarian cancer cell lines used in this study, except COV644 (Sigma®; St. Louis, Missouri, USA), were purchased from ATCC® (Manassas, Virginia, USA). Human Ovarian Surface Epithelial Cells (HOSEpiC) were used as non-cancerous control (ScienceCell™; Carlsbad, California, USA). SKOV-3 and OVCAR-3 were maintained in RPMI-1640 (ATCC®) supplemented with 20% fetal calf serum (FBS, HyClone™; Logan, Utah, USA) and 10 μg/ml of insulin solution from bovine pancreas (Sigma®). UACC-1598 and UWB1.289 were cultured in DMEM/F-12 + GlutaMAX™ (Thermo Scientific™, Austin, Texas, USA) (10% FBS), TOV112D and TOV21G were maintained in MCDB 105 + M199 (Sigma®) (15% FBS) and COV644 in DMEM+GlutaMAX™ (Thermo Scientific™) (10% FBS). HOSEpiC cells were cultured in Prigrow I (abm®; Richmond, Canada) supplemented with 0.01% ovarian epithelial cell growth supplement (ScienceCell™) (10% FBS) and grown in extracellular matrix coated-flasks (abm®). All cell lines were supplemented with penicillin [100 U/ml] and streptomycin [100 μg/ml] (Corning cellgro®; Manassas, Virginia, USA) and maintained at 37 °C in a humidified 5% $CO_2$ incubator. All cell lines used in this study were tested and resulted free of mycoplasma infections.

### *Antibodies*

The following commercial antibodies were used for immune blotting with the indicated dilutions: anti-HBO1 (1:1000, Abcam®; Cambridge, Massachusetts, USA), anti-GAPDH (1:2000, Santa Cruz®; Dallas, Texas, USA), anti-H4ac (1:1000, Active motif®; Carlsbad, California, USA), anti-H4 (1:1000, Active motif®), anti-H3K14ac (1:1000, Active motif®), anti-CyPA (1:200, Santa Cruz®), anti-XRCC1 (1:250, Santa Cruz®) and anti-EGFR (1:250, Santa Cruz®). Anti-HBO1 (1:100) and Alexa Fluor® 488 secondary antibody (1:500, Thermo Scientific™) were used for immune-fluorescence staining.

### *Total RNA extraction and qRT-PCR*

Total RNA was isolated with the RNeasy kit (Qiagen®; Germantown, Maryland, USA) and reverse transcribed to cDNA using SuperScript® II reverse transcriptase and random primers following the first-strand synthesis protocol (Thermo Scientific™). All qRT-PCR reactions were conducted in a LightCycler®480 II instrument (Roche, Indianapolis, Indiana, USA) using 2X SYBR Green I MasterMix. Relative gene expression was determined following the $\delta C_t$ method[26] and normalized to GAPDH expression. All samples were tested in duplicates. When possible, synthetic oligonucleotides (sequence available upon request) span exon-exon boundaries to preclude amplification of genomic DNA. ANOVA statistical analyses were performed on $\delta C_t$ values of three biological replicates using Graphpad Prism (V6); the Tukey's HSD test was used to correct for multiple comparison testing.

### *Protein extraction and western blot*

Cells were lysed using RIPA buffer (150 mM NaCl, 50 mM Tris pH 7.5, 0.5% sodium deoxycholate, 0.1% SDS, 1% Triton X-100, protease inhibitor cocktail [Roche]) and total protein was quantified using a standardized bovine serum albumin protein concentration curve following the Bio-Rad DC™ protein assay (Bio-Rad; Hercules, California, USA). Total protein samples (10 μg) were separated using SDS-PAGE and then transferred to a PVDF membrane. Primary antibody incubations were performed overnight

(O/N) followed by 2 hours in the presence of HRP-conjugated secondary antibodies. Protein intensity was detected with Luminata™ Classico HRP substrate (Millipore™; Temecula, California, USA). All western blots were performed three times and relative protein intensity levels were calculated using ImageJ.[27] The graphical depiction of relative protein levels represents the proportional difference between a treatment and its control (100%). ANOVA analyses were performed on relative intensity values using Graphpad Prism (V6); the Tukey's HSD test was used to correct for multiple comparison testing.

*Immunofluorescence and subcellular protein fractionation*

Cells were cultured in 4-well chamber slides (Nunc™ Lab-Tek™ II, Thermo Scientific™) and grown overnight at 37 °C. After this, cells were washed with PBS (HyClone™) twice and fixed with 3.7% formaldehyde (Sigma®). After several PBS washes, the cells were permeabilized with 0.25% Triton X-100, blocked for 1 h with 3% BSA in PBS and washed thoroughly in PBS again. Following this step, cells were incubated with the primary antibody diluted in blocking solution for 4 h in a dark humidified chamber (4 °C) and then with secondary antibody for 1 h in the same conditions. Slides were mounted with DAPI solution (Thermo Scientific™) as per manufacturer instructions and observed in a Nikon Eclipse Ti Microscope (Nikon®; Melville, New York, USA). Each experiment was repeated twice and one chamber slide containing target cells was incubated with the secondary antibody alone as auto-fluorescence control. The subcellular protein fractionation was performed three times following manufacturer's instructions (Thermo Scientific™). Cells were cultured in TC dishes (60x15mm, Falcon®; Greenwood, Indiana, USA), lysed with RIPA buffer and run in SDS-PAGE gels as indicated in the western blot section. Relative protein intensity, expressed as localization percentage, was calculated using ImageJ.[27]

*RNA interference*

Cells were cultured O/N in Costar® Clear TC-treated 12-well plates (Sigma®) in pertinent media without antibiotics. ON-TARGETplus Human KAT7 siRNA-SMART-pool (GE Dharmacon™; Lafayette, Colorado, USA) was used in order to transiently knockdown HBO1, while an ON-TARGETplus Non-targeting pool (GE Dharmacon™) was used as control (siRNA guide sequences can be found in the Supplementary Table S1). Cells were transfected with the siRNA pool [25 nM] or individual siRNAs [6.25 nM] using DharmaFECT Transfection Reagent (GE Dharmacon™) following manufacturer's instructions. Cells transfected with Transfection Reagent alone were used as non-siRNA control.

*Microarray hybridization and analysis*

Human whole genome expression arrays (HumanHT-12 v4) were purchased from Illumina® (San Diego, California, USA). Complementary RNA (cRNA) synthesis and labeling were performed as described previously.[28] Unmodified microarray data obtained from the GenomeStudio was background-subtracted and quantile-normalized using the lumi package[29] within R. To determine the effect of RNA interference, microarrays were analyzed using the two-class paired-rank product method[30,31] within the multiple array viewer (MEV). The analysis was corrected for multiple hypotheses testing and the siRNA effect was considered significant when the false discovery rate (FDR) fell below the 10% (FDR < 0.1). To facilitate comparisons among the datasets, all data was uploaded into an SQLite3 database. The Venn diagram was designed using the Venny website (http://bioinfogp.cnb.csic.es/tools/venny/; August 2018).

Table 1
Ovarian cancer and non-cancerous cell lines used in the study.

| Cell line | Histology | Grade | Stage |
|---|---|---|---|
| HOSEpiC | Ovarian surface epithelium | | |
| SKOV-3 | Serous | - | - |
| OVCAR-3 | High-grade serous | 3 | - |
| UWB1.289 | Serous | - | - |
| UACC-1598 | Serous | 3 | IV |
| TOV-112D | Endometrioid | 3 | IIIC |
| TOV-21G | Clear-cell | 3 | III |
| COV644 | Mucinous | - | - |

*Pathway analysis*

Ingenuity Pathway Analysis (IPA®, Qiagen®) was used to compare differentially expressed genes with thousands of curated datasets in order to perform functional analysis of the RNA silencing. Files containing differentially expressed genes with their associated fold-change values were uploaded to IPA®. These data was used to determine significantly affected pathways upon siRNA depletion (Canonical pathways) and to identify possible influenced downstream biological processes.

*Determination of viability, cell death and apoptosis*

The ApoTox-Glo™ triplex assay (Promega®, San Luis Obispo, California, USA) allows assessing of cell viability, cell death (cytotoxicity) and apoptosis (caspase activity) in the same experiment. This assay was performed following manufacturer's instructions. Substrates were always added to untreated wells and wells without cells as additional controls and all samples were tested in triplicates. The graphical depiction of relative cell viability, cytotoxicity and caspase activation represents the proportional difference between a treatment and its control (100%). ANOVA analyses were performed on raw values using Graphpad Prism (V6); the Tukey's HSD test was used to correct for multiple comparison testing.

*Lentiviral infection*

A set of three SMARTvector™ Lentiviral shRNA KAT7 particles (GE Dharmacon™) was purchased in order to constitutively knockdown HBO1. SMARTvector™ Non-targeting Lentivirus particles (GE Dharmacon™) were used as negative control (shRNA guide sequences can be found in the Supplementary Table S1). The protocol for transduction of lentiviral particles was performed following manufacturer's instructions. Cells were transduced with individual shRNAs supplemented with polybrene [10 μg/mL] (Santa Cruz®) for 6 h. The transduction medium was then replaced by normal growth medium, in which cells proliferated for 2 days. Next, cells

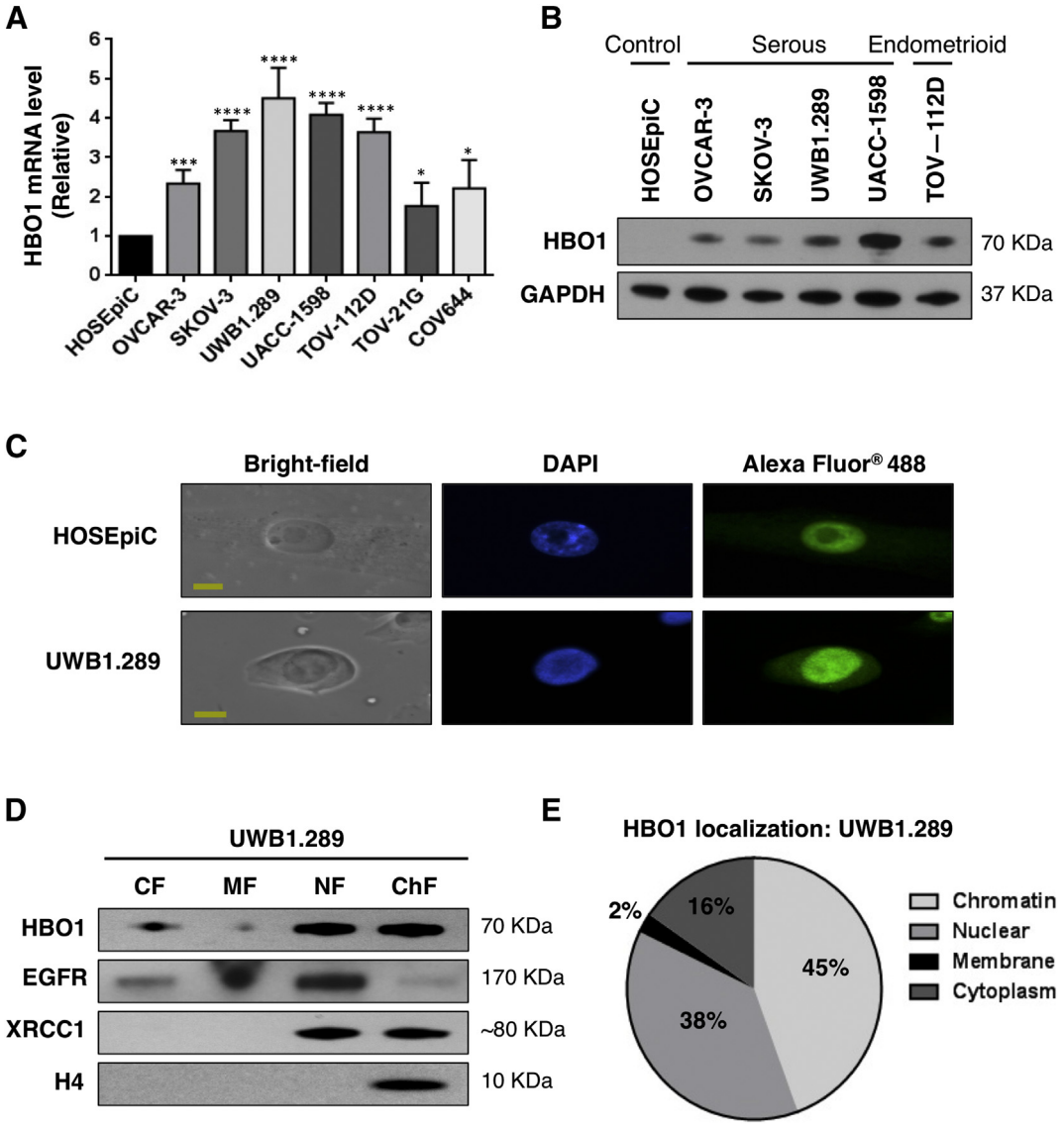


Figure 1. HBO1 is overexpressed in ovarian cancer cell lines. Cell lysates from 7 ovarian cancer cell lines and a non-cancerous control (HOSEpiC) were subjected to (**A**) qRT-PCR and (**B**) western blot analyses. All values represent the mean ± SD of at least three biological samples (*$P < 0.05$; ***$P < 0.001$; ****$P < 0.0001$). (**C**) Immune-fluorescence staining showing HBO1 localization in HOSEpiC and UWB1.289 cells. First column (Bright-field) displays optical microscopic images of cells; second (DAPI) and third (Alexa Fluor® 488) show fluorescent-labeled DNA and HBO1 images respectively. Scales represent 10 μm. (**D**) Subcellular protein fractionation of UWB1.289 cell lysates shows a nuclear distribution of HBO1 (~83% NF + ChF). CF: cytoplasm fraction, MF: membrane fraction, NF: nuclear fraction, ChF: chromatin fraction. EGFR, XRCC1 and Histone 4 antibodies were used as positive controls. (**E**) Pie chart showing the cellular distribution of HBO1 protein according to the subcellular protein fractionation. Immune-fluorescence and subcellular fractionation experiments were performed twice.

were cultured for 48 h in growth media containing puromycin [1 μg/mL] (Santa Cruz®), a period after which a lower concentration of puromycin [0.5 μg/mL] was added for another 48 h to reassure the selection of transduced cells. Finally, transduced cells were observed in a Nikon Eclipse Ti Microscope (Nikon®) to assess green fluorescent protein (GFP) expression.

*Atomic force microscopy*

Cells were analyzed using a BioScope Catalyst (Bruker Instruments; Santa Barbara, California, USA). Novascan borosilicate colloidal probes were used, with a sphere radius of 2.5 μm, spring constant 0.17 N/m and deflection sensitivity 20.11 nm/V, experimentally determined on a clean glass slide. A total of 40 cells per sample type were analyzed. Three force curves were acquired on the center of each cell, using a ramp size of 3.5 μm, a ramp speed of 1 Hz and an applied force of 400 pN. The region of contact in each approach curve was fitted with the Hertz model (Eq. (1), shown below) using the Nanoscope analysis software (V1.5).

$$F = \frac{4E\sqrt{R}\,\delta^{3/2}}{3\,(1-\upsilon^2)} \quad (1)$$

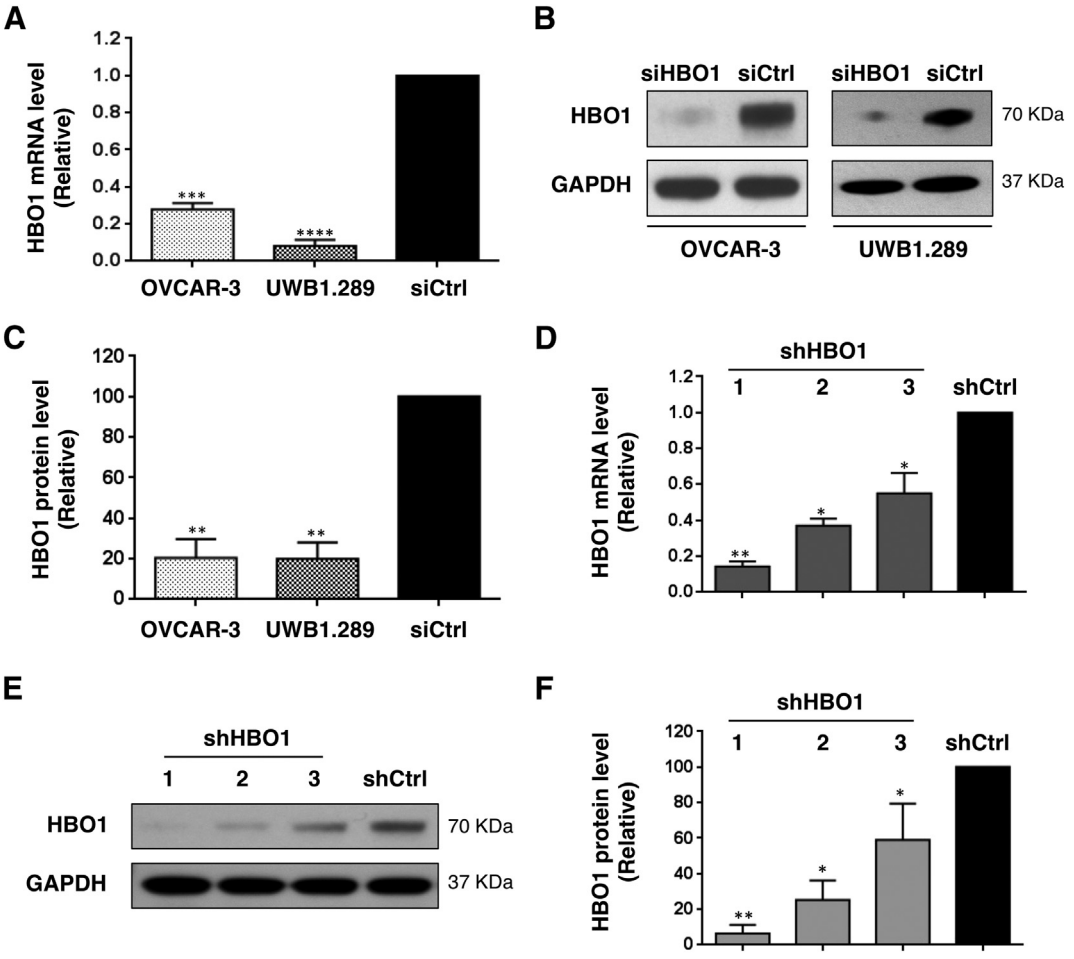


Figure 2. HBO1 knockdown resulted in significant mRNA and protein depletion. SiRNA-mediated knockdown in OVCAR-3 and UWB1.289 cells resulted in significant HBO1 (**A**) transcript and (**B**) protein reduction after 48 hours compared to the control treatment (siCtrl). (**C**) Proportional difference between relative densities of HBO1 protein in knockdown and control samples; relative densities were calculated using ImageJ. The transduction of three shRNAs (1–3) in UWB1.289 cells led to significant HBO1 (**D**) transcript and (**E**) protein reduction compared to the non-targeting control (shCtrl). (**F**) Proportional difference between relative densities of HBO1 protein in knockdown and control samples; relative densities were calculated using ImageJ. All values represent the mean ± SD of three biological samples (*$P < 0.05$; **$P < 0.01$; ***$P < 0.001$; ****$P < 0.0001$).

In Eq. (1), $F$ is the force applied by the cantilever tip to the cell, $E$ is the Young's modulus (fit parameter), υ is the Poisson ratio (0.5), $R$ the radius of the indenter (2.5 μm) and δ the indentation of the cell. Only data displaying a goodness-of-fit higher than 0.9 was taken into consideration. Each retraction curve was analyzed for the presence of adhesion events. Data distribution and statistical analysis were performed using Wolfram Mathematica 10 and Minitab (V17). Mann–Whitney test was used to assess statistical significance between data population.

### *Accession numbers*

Raw microarray data has been deposited in the Gene Expression Omnibus (GEO) database of the NCBI (https://www.ncbi.nlm.nih.gov/gds). GEO accession number **GSE89922** corresponds to the UWB1.289 microarray and GEO accession number **GSE89359** to the OVCAR-3 microarray.

## Results

### *HBO1 is highly expressed in ovarian cancer cell lines*

HBO1 expression levels were determined in a panel of OC cell lines (Table 1). HGSC OC cells (OVCAR-3, SKOV-3, UWB1.289 and UACC-1598) expressed significantly higher HBO1 mRNA relative to the non-cancerous ovarian epithelial cell control (HOSEpiC) (Figure 1, *A*). Significantly higher expression levels were also detected in the endometrioid line TOV-112D. Western blot analysis determined that elevated transcript levels were accompanied by concomitant increases in HBO1 protein (Figure 1, *B*).

HBO1 subcellular localization was determined in UWB1.289 using immunofluorescence staining, and, as expected, found to be nuclear, evenly distributed throughout the nucleoplasm and excluded from the nucleoli (Figure 1, *C*). This distribution was similar, but weaker, in HOSEpiC cells (Figure 1, *C*). Subcellular fractionation experiments further confirmed HBO1 was predominantly nuclear localized, and that a significant fraction of HBO1

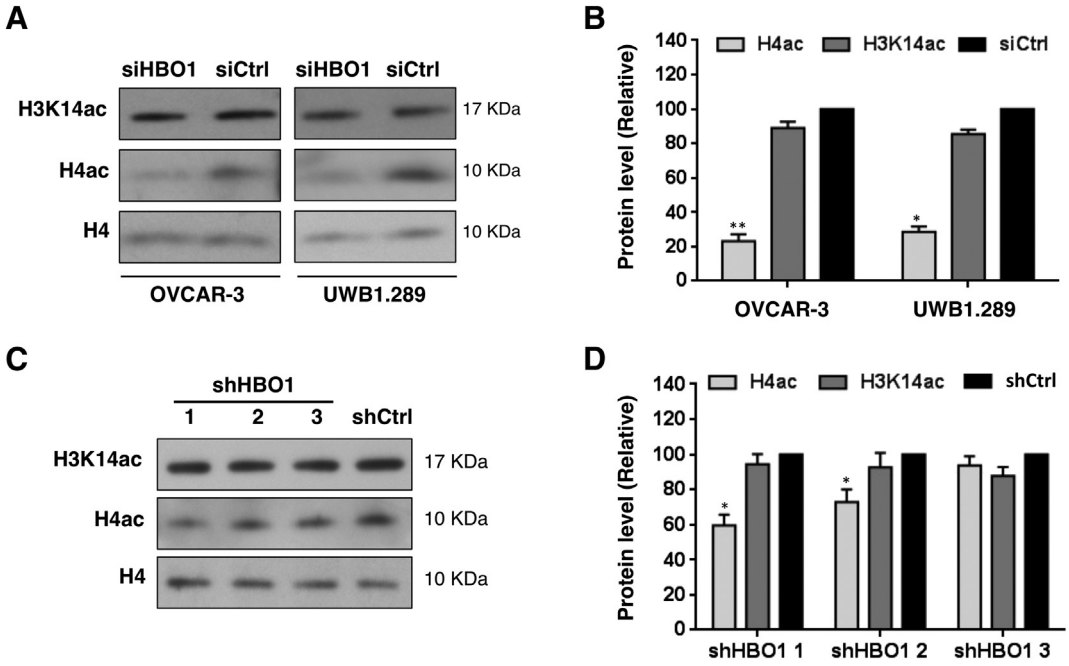


Figure 3. HBO1 directs histone H4 acetylation in ovarian cancer cells. (**A**) HBO1 knockdown reduced bulk histone H4 acetylation in OVCAR-3 and UWB1.289 cells compared to the control treatment (siCtrl), however H3K14 acetylation remained unchanged after 48 h. (**B**) Proportional differences of acetylated H4 and acetylated H3K14 compared to the histone 4 controls after transient HBO1 knockdown. (**C**) Stable knockdown of HBO1 using three shRNAs (1–3) reduced bulk histone H4 acetylation when compared to the non-targeting control (shCtrl), while no effect was observed in H3K14 acetylation. (**D**) Proportional differences of acetylated H4 and acetylated H3K14 compared to the histone 4 controls after stable HBO1 knockdown. All values represent the mean ± SD of three biological samples (*$P < 0.05$; **$P < 0.01$).

is present in the same cellular fraction as chromatin, represented by the histone H4 control (Figure 1, *D* and *E*). Thus, HBO1 is highly expressed in serous OC cell lines versus the non-cancerous control and displays normal nuclear localization in this context.

### *HBO1 is required for histone H4 but not H3K14 acetylation*

To understand the function(s) of HBO1 in OC cells, we performed transient siRNA transfection into OVCAR-3 and UWB1.289 cells. Optimal KD was obtained 48 hours after siRNA transfection (Supplementary Figure S1), and this treatment led to substantial decreases in steady state HBO1 transcript (70–90%, Figure 2, *A*) and protein (60–80%, Figure 2, *B* and *C*). Furthermore, a stable HBO1 knockdown cell line was generated using lentiviral transduction of three different shRNAs in UWB1.289 cells. This approach also rendered a significant stable reduction in the expression of HBO1 transcript (50–90%) and protein (40–90%) (Figure 2, *D–F*). Both transient and stable HBO1 KD revealed no obvious changes in cell morphology or replication rate when analyzed through the use of light microscopy and raw cell count respectively (not shown).

Using the HBO1 KD models we analyzed the levels of acetylation of defined HBO1 histone targets, H4 (using a pan-H4 antibody to simultaneously analyze H4K5, 8, 12 and 16) and H3K14. Transient HBO1 KD resulted in reduction in bulk H4 acetylation in OVCAR-3 and UWB1.289 OC cells (Figure 3, *A* and *B*), however H3K14 acetylation was unchanged (Figure 3, *A* and *B*), suggesting that HBO1 is primarily involved in H4 acetylation in OC cells, and that targeting of H3K14 by HBO1 may be limited to very specific developmental stages and cell types, as observed in pre-gastrulation mouse embryos.[5,6] Similarly, stable HBO1 KD also resulted in reduced acetylation of histone H4 (Figure 3, *C* and *D*) and not H3K14 acetylation (Figure 3, *C* and *D*). Together these results suggest that HBO1 has a selective role in maintaining H4 acetylation in OC cell lines.

### *HBO1-complex components are overexpressed in ovarian cancer cell lines*

The specificity observed towards H4 acetylation may be due to the molecular composition and therefore selectivity of the HBO1-complex in OC cells, accordingly the relative expression levels of HBO1-complex cofactors ING4/5, BRPF1/2/3 and JADE1/2/3 was determined (Figure 4, *A–C*). In OVCAR-3, ING5 expression was approximately 2/3-fold at higher levels than controls (Figure 4, *A*). BRPF1 was elevated 1.5/2-fold in both cell lines (Figure 4, *B*). However, JADE2 and JADE3 were very highly expressed in OC cells, with exceptionally high levels of JADE2 transcript present in UWB1.289 cells (~10-fold greater than controls) (Figure 4, *C*). These observations suggest that whilst HBO1 could be present in a number of different complexes, it is likely that a JADE2/3-associated complex is the most predominant in OC cells. This HBO1-JADE complex offers an explanation for the histone H4 specificity of HBO1 observed in these cells.[14]

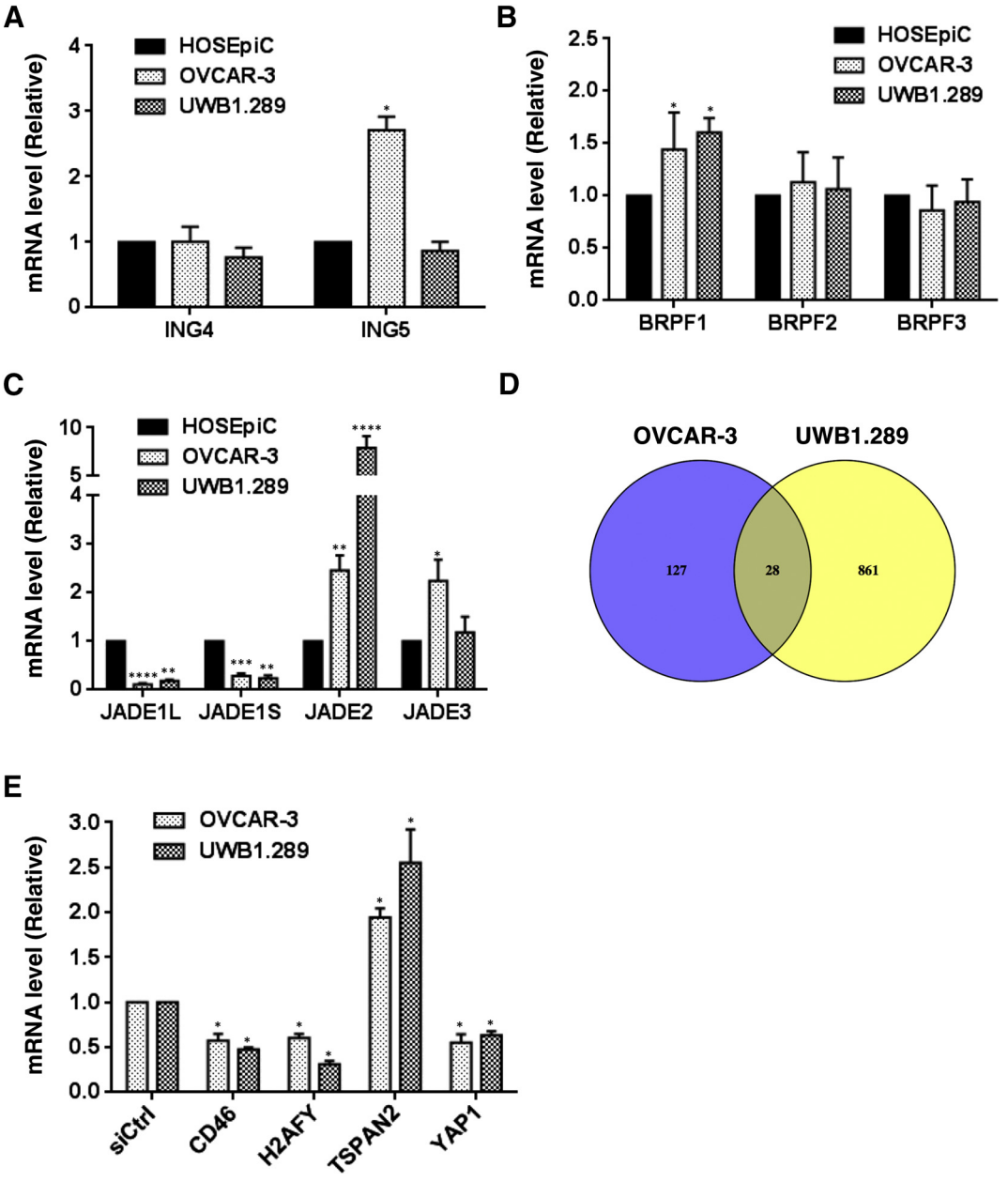


Figure 4. Expression levels of the HBO1-complex regulate important subsets of genes in ovarian cancer cell lines. (**A**) Inhibitor of growth (ING) tumor suppressor proteins 4/5 mRNA expression level in OVCAR-3 and UWB1.289 cells compared to the non-cancerous control (HOSEpiC). (**B**) Scaffolding subunits BRPF1/2/3 mRNA expression level comparison. (**C**) Scaffolding subunits JADE1/2/3 mRNA expression level comparison. (**D**) Venny depiction of HBO1-regulated genes in OVCAR-3 and UWB1.289 cell lines following transient depletion of HBO1 (48 h). (**E**) qRT-PCR validation of HBO1-associated genes in HBO1 knockdown lysates of OVCAR-3 and UWB1.289 cells. All values represent the mean ± SD of three biological samples (*$P < 0.05$, **$P < 0.01$; ***$P < 0.001$, ****$P < 0.0001$).

*HBO1 knockdown results in specific gene expression changes in ovarian cancer cells*

We assessed gene expression changes after transient HBO1 KD in the two OC cell lines via microarray. Global transcriptome analyses revealed a number of differentially regulated HBO1-dependent genes in UWB1.289 (Table 2 and Supplementary Table S2) and OVCAR-3 (Table 2 and Supplementary Table S3), and were validated by qRT-PCR analysis (Supplementary Figure S2). The initial siRNA KD system used in these experiments utilized a pool of four distinct siRNA, therefore individual HBO1 siRNAs were also used to validate the observed effect (Supplementary Figure S3). Comparative analysis between OVCAR-3 and UWB1.289 gene lists identified an 'HBO1 signature' gene set (Figure 4, *D* and Table 2), from which selected targets were verified by qRT-PCR analysis.

Table 2
Common gene expression changes caused by HBO1 knockdown in OVCAR-3 and UWB1.289 cell lines.

| Gene | Fold-change OVCAR-3 | Fold-change UWB1.289 |
|---|---|---|
| OAS2 | 4.15 | 1.75 |
| IFIT1 | 3.25 | 1.64 |
| CXCL10 | 3.18 | 1.55 |
| IFIT2 | 2.54 | 1.52 |
| OASL | 2.02 | 1.53 |
| MX1 | 1.76 | 1.50 |
| IRF9 | 1.74 | 1.52 |
| GBP5 | 1.60 | 2.04 |
| TSPAN2 | 1.59 | 1.50 |
| GBP1 | 1.58 | 1.81 |
| RASSF2 | 1.52 | 1.88 |
| TLE4 | 1.51 | 1.50 |
| MAP2 | 1.50 | 2.35 |
| CDR2 | −1.50 | −1.95 |
| RNF141 | −1.50 | −1.52 |
| AGFG1 | −1.52 | −1.51 |
| MYST2 | −1.54 | −2.70 |
| RABL2A | −1.55 | −2.09 |
| H2AFY | −1.55 | −2.13 |
| TNFRSF10D | −1.55 | −2.00 |
| S100A2 | −1.56 | −1.74 |
| CHORDC1 | −1.57 | −2.60 |
| CD46 | −1.62 | −1.81 |
| RABL2B | −1.64 | −2.04 |
| C3orf64 | −1.73 | −1.83 |
| SMPDL3B | −1.79 | −1.63 |
| ADRB2 | −1.96 | −1.87 |
| LOC648927 | −2.09 | −4.01 |

CD46, H2AFY and YAP1 genes were significantly down-regulated, and TSPAN2 was significantly up-regulated in both cell lines (Figure 4, *E*).

*HBO1 knockdown increases cell viability in vitro*

Bioinformatic analysis of HBO1 target gene function predicted an association with enhanced cellular movement, migration, invasion and reduced cell death (Supplementary Table S4). Whereas measurements for gross cellular activities, including invasion, proliferation and wound-healing assays did not reveal any functional changes upon HBO1 KD (Supplementary Figure S4, *A–C*), increased cell viability was observed (Figure 5, *A*). This effect was accompanied with a significant reduction in apoptosis, as determined by measurement of gross caspase activity (Figure 5, *B*) and in cell cytotoxicity (Figure 5, *C*). Transient HBO1 KD also resulted in reduced levels of CypA/PPIA, a marker of cell death (Figure 5, *D* and *E*).[32] Stable knockdown of HBO1 using shHBO1 displayed similar increases in viability (Figure 5, *F*).

*HBO1 stable knockdown reduces cell membrane elasticity in UWB1.289 cells*

The increased cell viability observed following loss of HBO1, and the lack of effect on general processes involved in cancer phenotypes, led us to ask whether HBO1 might be involved in the regulation of more subtle oncogenic transformation processes such as cytoskeletal reorganization, as has been recently reported for cellular transformation involved in endometrial desidualization, a process similar to mesenchymal-to-endothelial transitions (MET).[33] AFM was used to investigate the surface biomechanical properties in UWB1.289 cells (Figure 6, *A* and *B*). 2.5 μm radius spherical (colloidal) probes, which are suited to inspect overall cellular surface changes rather than local nanoscopic differences,[34] were used to interrogate cell properties including stiffness and adhesiveness. Approach force curves were used to extract specific Young's modulus (Figure 6, *C* and *D*), and the Hertz equation used to fit the contact regime of each approach curve (Eq. (1) in Methods) and demonstrated an excellent goodness of fit (89% > 0.9).

A Young's modulus of 294 ± 14 Pa was measured in cells expressing normal HBO1 levels, which increased to 397 ± 17 Pa when HBO1 expression was reduced (Figure 6, *E*), suggesting that HBO1 is involved in promoting a less organized/differentiated and more elastic phenotype in OC cells, a common characteristic of invasive tumor cells.[35] Consistently, previous AFM data demonstrated that the highly metastatic ovarian cancer cell line HEY A8 displayed a Young's modulus of 490 ± 220 Pa, compared to its less aggressive counterpart HEY, where elasticity was measured as 880 ± 530 Pa.[36] Surface adhesiveness was evaluated through measuring the force needed to detach the spherical probe from the cell surface during a retracting cycle as indicated in Figure 6, *F*. In this case, the median adhesion values for the control and transformed cells were not significantly different ($P > 0.05$; 38 ± 2 pN and 39 ± 2 pN).

Cellular elastic properties, known to determine and characterize functional phenotypes in OC development, are linked to intrinsic gene regulatory processes including YAP1 pathways.[36,37] Overexpression of YAP1, a main downstream nuclear effector of the Hippo signaling pathway, has been reported in OC,[38,39] where it is thought to act as an oncogene associated with aggressive disease and poor prognosis.[40,41] Importantly, YAP1 is also widely regarded as a mechano-transducer, as its transcriptional activity is responsive to a complex array of mechanical and geometric cues.[42] YAP1 is one of the main target effectors regulated by HBO1, as seen previously in OVCAR-3 and UWB1.289 cells (Figure 4, *E*) and other OC cell lines including TOV-112D, UACC-1598 and SKOV-3 (Supplementary Figure S5). These results suggest that HBO1 influences the mechano-phenotype of OC cells shaping their elasticity, and responsiveness to mechanical perturbations via the regulation of YAP1 expression.

## Discussion

HGSC is the most common and aggressive OC histo-type and, with the exception of poly (ADP-ribose) polymerase inhibitors in patients with BRCA1/2 mutations,[43] existing therapies ultimately yield disappointing results. Identification of target molecules with key roles in HGSC phenotype and progression could facilitate the development of new therapies. Since HBO1 is overexpressed in serous OC,[4] and appears important in cancer proliferation,[44] we sought to determine the role of HBO1 in OC.

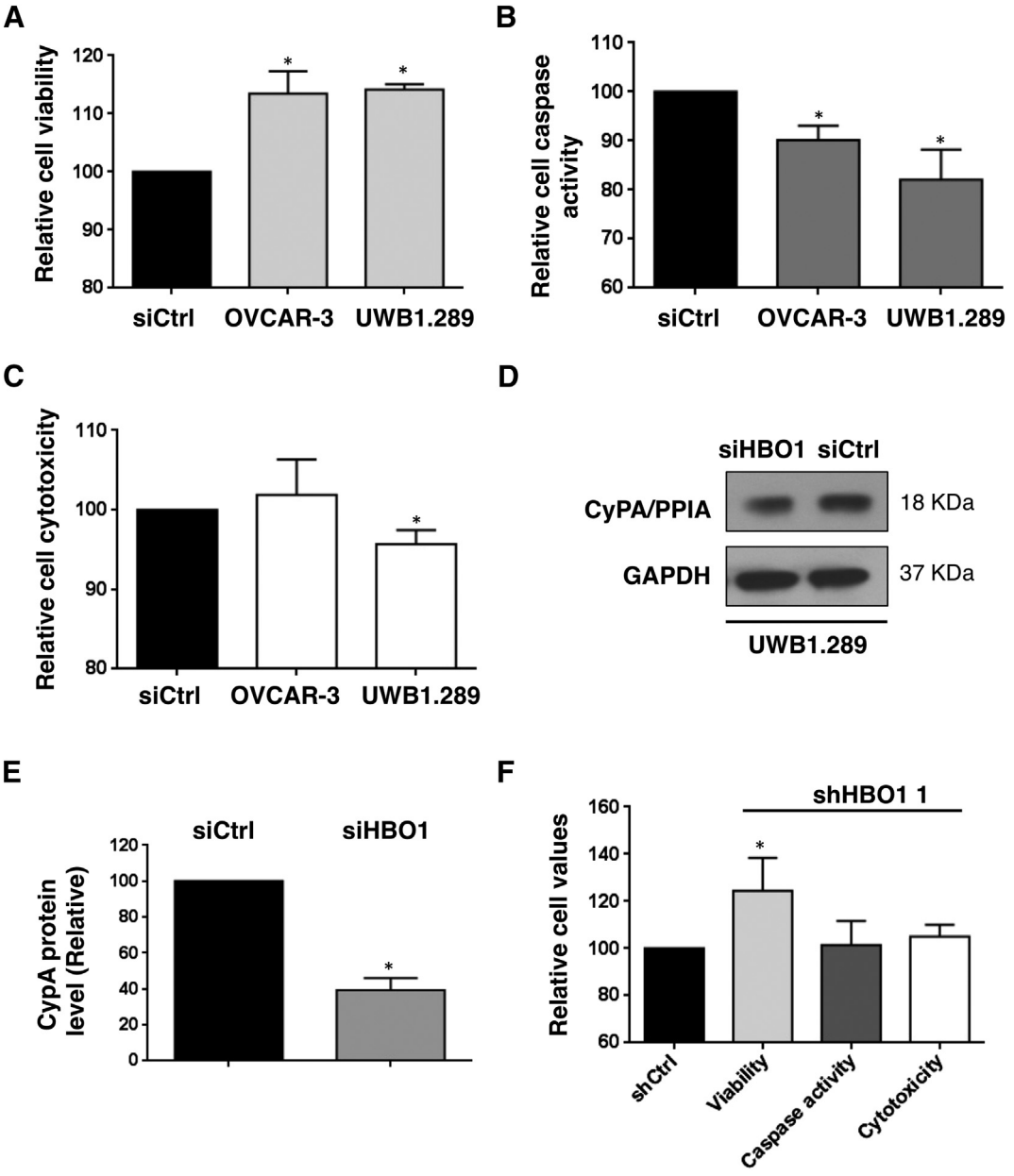


Figure 5. HBO1 regulates cell viability and apoptosis in vitro. After HBO1 knockdown, OVCAR-3 and UWB1.289 cells were subjected to (**A**) Viability, (**B**) Apoptosis (caspase activation) and (**C**) Cytotoxicity assays. The graphical representations display the proportional difference between HBO1 knockdown and control measurements (siCtrl). Each HBO1 knockdown was compared to their correspondent cell line control sample but only one control was plotted in order to simplify the images. (**D**) siRNA-mediated HBO1 knockdown led to a significant reduction in CypA/PPIA protein levels in UWB1.289 after 48 h. (**E**) Proportional difference between relative densities of CypA/PPIA protein in knockdown and control samples; relative densities were calculated using ImageJ. (**F**) UWB1.289 cells expressing shHBO1 1 and the non-targeting control (shCtrl) were subjected to viability, caspase activity and cytotoxicity assays. The graphical representation displays the proportional difference between HBO1 knockdown and control measurements. The value of each assay was compared to its correspondent control but only one was plotted in order to simplify the image. All values represent the mean ± SD of three biological samples (*$P < 0.05$).

All serous-like OC cell lines evaluated expressed high levels of HBO1 relative to controls, with highest levels of HBO1 transcript observed in UACC-1598 and TOV-112D, which were isolated from patients with late stages of disease (IV and IIIC respectively). Interestingly, TOV-112D is derived from an endometrioid carcinoma that shares similarities with HGSCs.[45]

HBO1 was required for bulk histone H4 acetylation but had no effect on the acetylation status of H3K14, suggesting that in OC overexpression of HBO1 may result in a specific acetylation function. Loss of HBO1 was not accompanied by any compensatory overexpression of other HATs. In fact, PCAF/KAT2B, previously linked to enhanced rates of DNA replication,[46] was down-regulated when HBO1 was knocked-down. The specificity observed for H4 acetylation is likely due to the overexpression of JADE2/3 HBO1 HAT-complex components. The composition of the HBO1 complex has been proposed

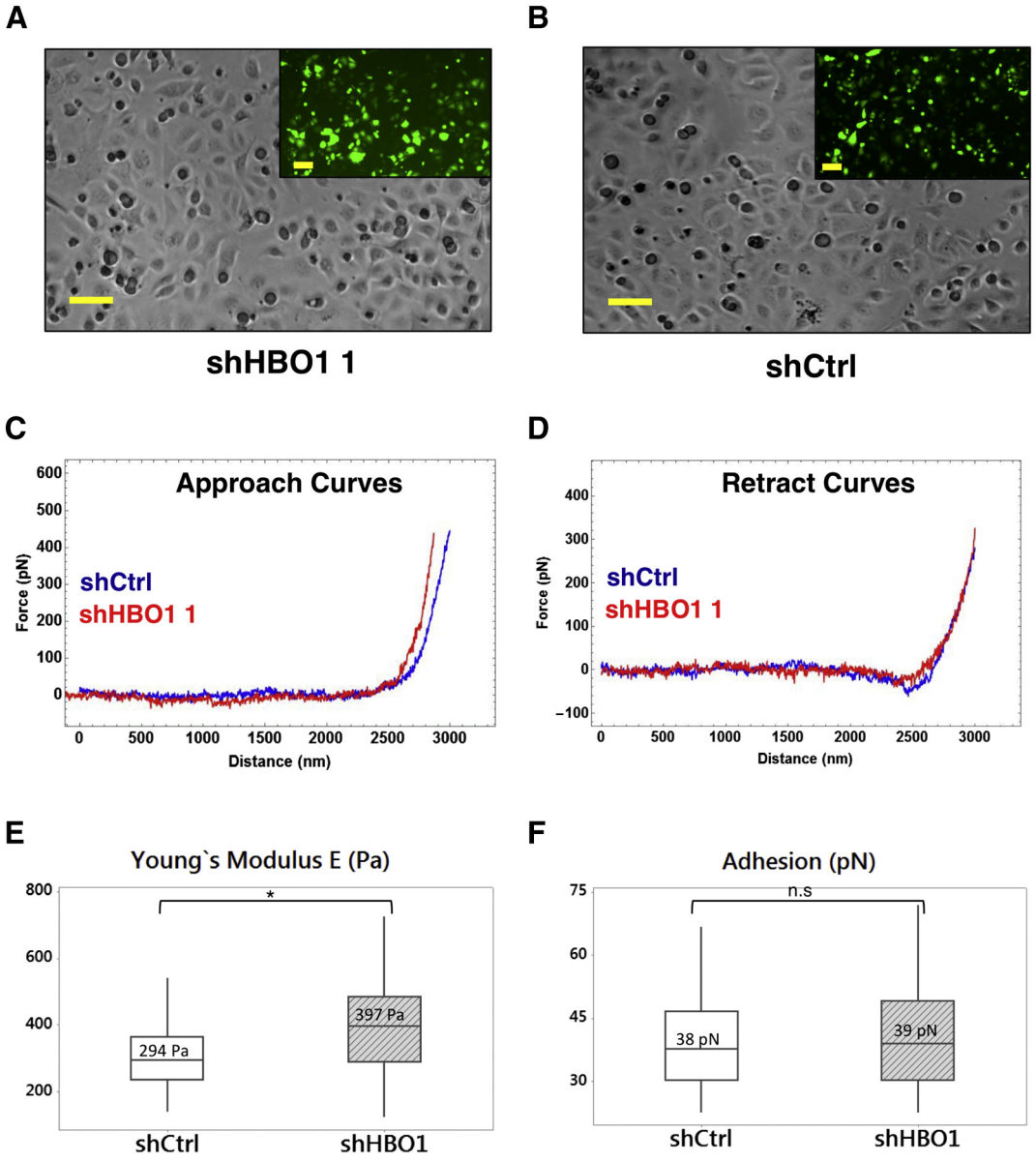


Figure 6. Stable HBO1 knockdown significantly increases the Young modulus of UWB1.289 cell membrane. UWB1.289 cells transduced with lentiviral constructions targeting (**A**) HBO1 and (**B**) non-targeting control (shCtrl) displayed normal morphology and expressed high levels of green fluorescent protein (GFP) linked to shRNA production. Examples of (**C**) approach and (**D**) retract Atomic Force Microscopy (AFM) curves applied onto UWB1.289 cells. (**E**) Stable knockdown of HBO1 (shHBO1 1) led to a significant increase in membrane tension compared to the control: 397 ± 17 Pa and 294 ± 14 Pa, respectively (*$P < 0.05$). (**F**) Surface adhesiveness for shHBO1 1, 39 ± 2 pN, was not significantly different from shCtrl, 38 ± 2 pN (n.s.: not significant).

as a mechanism of switching HAT activity from one histone target to the other (H3-H4),[14] thus specifically modulating cell functionality, and JADE containing HBO1-complexes appear to direct HBO1 activity towards histone H4. High levels of JADE2 expression may also have prevented anti-HBO1 antibodies recognizing HBO1 in genome wide chromatin immune-precipitation (ChIP) analysis due to the proposed alteration in the stoichiometry of the HBO1-JADE2 complex.

Transcriptome analysis following depletion of HBO1 in OC cells, in general, pointed to multiple oncogenic roles for HBO1. CD46, a complement inhibitor involved in the protection of tumor cells against the host immune system, was down-regulated following HBO1 depletion, which is consistent with previous studies that reported overexpression in OC tissues, links to shorter survival and poor prognosis.[47,48] YAP1, a well-known OC oncogene and mechano-transducer, was down-regulated in all tested OC cell lines after HBO1 knockdown, suggesting an underlying association between epigenome modulation and cell biomechanics.[49] However, HBO1 also displayed anti-cancer activities in OC cells, as we observed augmentation of cell viability without changes in cell proliferation following HBO1 knockdown. While it may be surprising that overexpression of HBO1 is associated with anti-oncogenic activities, there are precedents for this phenomenon in other cancer cell types, e.g.

the transcription factor NR2F2 is overexpressed in breast cancer, yet NR2F2 knockdown in MDAMB231 and MCF-7 breast cancer cells led to enhanced migration and invasion without changes in proliferation.[50]

Recent studies have revealed four strong gene expression subtypes in HGSC, termed immunoreactive, differentiated, proliferative and mesenchymal.[25] While these subgroups were not associated with obvious changes in overall survival, their existence may indicate that different approaches are needed to combat individual OC subtypes. Our genome wide pathway analysis data revealed that loss of HBO1 function overlaps with the OC mesenchymal signature, including increased cell survival, migration, cytoskeletal organization and microtubule dynamics. It is therefore interesting to consider the possibility that HBO1 overexpression suppresses the mesenchymal phenotype to favor others.

Whilst reduction in HBO1 expression did not appear to have any significant effect on proliferation, migration or invasion in OC cells, a significant decrease in cell elasticity, which is commonly associated with aggressive cancer phenotypes, was observed.[51] Differences in cell elasticity have been reported between non-malignant and ovarian cancer cells using AFM, where higher levels of membrane elasticity have been correlated to both high migratory and invasive activity.[36] The cell cytoskeleton has a central role in cell structure and intracellular organization, and thus affects cell mechanical properties that ultimately dictate cell functionality.[51] Interestingly, as cells transform from non-malignant to cancerous states, their cytoskeletal structure changes from an organized to an irregular network, reducing cell stiffness thus stimulating a more 'elastic' phenotype. Accordingly, cancer cells are softer and more deformable, which eventually leads to increased ability to infiltrate tissues and spread.[52] Reduction of HBO1 expression resulted in a significant decrease in cell membrane elasticity, a feature that is consistent with an aggressive cancer phenotype.[51] Direct comparison of the measured Young's modulus for UWB1.289 (this study) and the highly invasive HEY A8 cells,[36] suggests that UWB1.289 could be a more aggressive ovarian cancer cell type as it has higher membrane elasticity. These findings, together with the identification of a mechano-transducer as a major HBO1 target, suggest that this HAT regulates different molecular mechanisms that effectively influence OC biomechanics.

## Appendix A. Supplementary data

Supplementary data to this article can be found online at https://doi.org/10.1016/j.nano.2019.01.017.

## References


1. Brien GL, Valerio DG, Armstrong SA. Exploiting the epigenome to control Cancer-promoting gene-expression programs. *Cancer Cell* 2016;**29**:464-76.
2. Avvakumov N, Côté J. The MYST family of histone acetyltransferases and their intimate links to cancer. *Oncogene* 2007;**26**:5395-407.
3. Doyon Y, Cayrou C, Ullah M, Landry A-J, Côté V, Selleck W, et al. ING tumor suppressor proteins are critical regulators of chromatin acetylation required for genome expression and perpetuation. *Mol Cell* 2006;**21**:51-64.
4. Iizuka M, Takahashi Y, Mizzen CA, Cook RG, Fujita M, Allis CD, et al. Histone acetyltransferase Hbo1: catalytic activity, cellular abundance, and links to primary cancers. *Gene* 2009;**436**:108-14.
5. Kueh AJ, Dixon MP, Voss AK, Thomas T. HBO1 is required for H3K14 acetylation and normal transcriptional activity during embryonic development. *Mol Cell Biol* 2011;**31**:845-60.
6. Mishima Y, Miyagi S, Saraya A, Negishi M, Endoh M, Endo TA, et al. The Hbo1-Brd1/Brpf2 complex is responsible for global acetylation of H3K14 and required for fetal liver erythropoiesis. *Blood* 2011;**118**:2443-53.
7. Avvakumov N, Lalonde M-E, Saksouk N, Paquet E, Glass KC, Landry A-J, et al. Conserved molecular interactions within the HBO1 acetyltransferase complexes regulate cell proliferation. *Mol Cell Biol* 2012;**32**:689-703.
8. Wright DG, Marchal C, Hoang K, Ankney JA, Nguyen ST, Rushing AW, et al. Human T-cell leukemia virus type-1-encoded protein HBZ represses p53 function by inhibiting the acetyltransferase activity of p300/CBP and HBO1. *Oncotarget* 2016;**7**:1687-706.
9. Georgiakaki M, Chabbert-Buffet N, Dasen B, Meduri G, Wenk S, Rajhi L, et al. Ligand-controlled interaction of histone acetyltransferase binding to ORC-1 (HBO1) with the N-terminal transactivating domain of progesterone receptor induces steroid receptor coactivator 1-dependent coactivation of transcription. *Mol Endocrinol* 2006;**20**:2122-40.
10. Miotto B, Struhl K. Differential gene regulation by selective association of transcriptional coactivators and bZIP DNA-binding domains. *Mol Cell Biol* 2006;**26**:5969-82.
11. Sharma M, Zarnegar M, Li X, Lim B, Sun Z. Androgen receptor interacts with a novel MYST protein, HBO1. *J Biol Chem* 2000;**275**:35200-8.
12. Contzler R, Regamey A, Favre B, Roger T, Hohl D, Huber M. Histone acetyltransferase HBO1 inhibits NF-kappaB activity by coactivator sequestration. *Biochem Biophys Res Commun* 2006;**350**:208-13.
13. Saksouk N, Avvakumov N, Champagne KS, Hung T, Doyon Y, Cayrou C, et al. HBO1 HAT complexes target chromatin throughout gene coding regions via multiple PHD finger interactions with histone H3 tail. *Mol Cell* 2009;**33**:257-65.
14. Lalonde M-E, Avvakumov N, Glass KC, Joncas F-H, Saksouk N, Holliday M, et al. Exchange of associated factors directs a switch in HBO1 acetyltransferase histone tail specificity. *Genes Dev* 2013;**27**:2009-24.
15. Clark J, Edwards S, John M, Flohr P, Gordon T, Maillard K, et al. Identification of amplified and expressed genes in breast cancer by comparative hybridization onto microarrays of randomly selected cDNA clones. *Genes Chromosomes Cancer* 2002;**34**:104-14.
16. Pollack JR, Sørlie T, Perou CM, Rees CA, Jeffrey SS, Lonning PE, et al. Microarray analysis reveals a major direct role of DNA copy number alteration in the transcriptional program of human breast tumors. *Proc Natl Acad Sci U S A* 2002;**99**:12963-8.
17. Iizuka M, Susa T, Takahashi Y, Tamamori-Adachi M, Kajitani T, Okinaga H, et al. Histone acetyltransferase Hbo1 destabilizes estrogen receptor α by ubiquitination and modulates proliferation of breast cancers. *Cancer Sci* 2013;**104**:1647-55.
18. Zou C, Chen Y, Smith RM, Snavely C, Li J, Coon TA, et al. SCF (Fbxw15) mediates histone acetyltransferase binding to origin recognition complex (HBO1) ubiquitin-proteasomal degradation to regulate cell proliferation. *J Biol Chem* 2013;**288**:6306-16.
19. Sauer T, Arteaga MF, Isken F, Rohde C, Hebestreit K, Mikesch J-H, et al. MYST2 acetyltransferase expression and histone H4 lysine acetylation are suppressed in AML. *Exp Hematol* 2015;**43**:794-802.e4.
20. Vaughan S, Coward JI, Bast RC, Berchuck A, Berek JS, Brenton JD, et al. Rethinking ovarian cancer: recommendations for improving outcomes. *Nat Rev Cancer* 2011;**11**:719-25.
21. Siegel RL, Miller KD, Jemal A. Cancer statistics, 2016. *CA Cancer J Clin* 2016;**66**:7-30.
22. Prat J. Ovarian carcinomas: five distinct diseases with different origins, genetic alterations, and clinicopathological features. *Virchows Arch* 2012;**460**:237-49.

23. Ahmed AA, Etemadmoghadam D, Temple J, Lynch AG, Riad M, Sharma R, et al. Driver mutations in TP53 are ubiquitous in high grade serous carcinoma of the ovary. *J Pathol* 2010;**221**:49-56.
24. Berns EMJJ, Bowtell DD. The changing view of high-grade serous ovarian cancer. *Cancer Res* 2012;**72**:2701-4.
25. Network CGA. Integrated genomic analyses of ovarian carcinoma. *Nature* 2011;**474**:609-15.
26. Yuan JS, Reed A, Chen F, Stewart CN. Statistical analysis of real-time PCR data. *BMC Bioinformatics* 2006;**7**:85.
27. Schneider CA, Rasband WS, Eliceiri KW. NIH image to ImageJ: 25 years of image analysis. *Nat Methods* 2012;**9**:671-5.
28. Suh JH, Sieglaff DH, Zhang A, Xia X, Cvoro A, Winnier GE, et al. SIRT1 is a direct coactivator of thyroid hormone receptor β1 with gene-specific actions. *PLoS One* 2013;**8**e70097.
29. Du P, Kibbe WA, Lin SM. lumi: a pipeline for processing Illumina microarray. *Bioinformatics* 2008;**24**:1547-8.
30. Breitling R, Armengaud P, Amtmann A, Herzyk P. Rank products: a simple, yet powerful, new method to detect differentially regulated genes in replicated microarray experiments. *FEBS Lett* 2004;**573**:83-92.
31. Koziol JA. Comments on the rank product method for analyzing replicated experiments. *FEBS Lett* 2010;**584**:941-4.
32. Christofferson DE, Yuan J. Cyclophilin a release as a biomarker of necrotic cell death. *Cell Death Differ* 2010;**17**:1942-3.
33. Pan-Castillo B, Gazze SA, Thomas S, Lucas C, Margarit L, Gonzalez D, et al. Morphophysical dynamics of human endometrial cells during decidualization. *Nanomedicine* 2018;**14**:2235-45.
34. Carl P, Schillers H. Elasticity measurement of living cells with an atomic force microscope: data acquisition and processing. *Pflügers Arch* 2008;**457**:551-9.
35. Lekka M. Discrimination between Normal and cancerous cells using AFM. *Bionanoscience* 2016;**6**:65-80.
36. Xu W, Mezencev R, Kim B, Wang L, McDonald J, Sulchek T. Cell stiffness is a biomarker of the metastatic potential of ovarian Cancer cells. *PLoS One* 2012;**7**e46609.
37. McKenzie AJ, Hicks SR, Svec KV, Naughton H, Edmunds ZL, Howe AK. The mechanical microenvironment regulates ovarian cancer cell morphology, migration, and spheroid disaggregation. *Sci Rep* 2018;**8**:7228.
38. Steinhardt AA, Gayyed MF, Klein AP, Dong J, Maitra A, Pan D, et al. Expression of yes-associated protein in common solid tumors. *Hum Pathol* 2008;**39**:1582-9.
39. Moroishi T, Hansen CG, Guan K-L. The emerging roles of YAP and TAZ in cancer. *Nat Rev Cancer* 2015;**15**:73-9.
40. Zhang X, George J, Deb S, Degoutin JL, Takano EA, Fox SB, et al. The hippo pathway transcriptional co-activator, YAP, is an ovarian cancer oncogene. *Oncogene* 2011;**30**:2810-22.
41. Xia Y, Chang T, Wang Y, Liu Y, Li W, Li M, et al. YAP promotes ovarian cancer cell tumorigenesis and is indicative of a poor prognosis for ovarian cancer patients. *PLoS One* 2014;**9**e91770.
42. Panciera T, Azzolin L, Cordenonsi M, Piccolo S. Mechanobiology of YAP and TAZ in physiology and disease. *Nat Rev Mol Cell Biol* 2017;**18**:758-70.
43. Symeonides S, Gourley C. Ovarian Cancer molecular stratification and tumor heterogeneity: a necessity and a challenge. *Front Oncol* 2015;**5**:229.
44. Duong MT, Akli S, Macalou S, Biernacka A, Debeb BG, Yi M, et al. Hbo1 is a cyclin E/CDK2 substrate that enriches breast cancer stem-like cells. *Cancer Res* 2013;**73**:5556-68.
45. Köbel M, Kalloger SE, Carrick J, Huntsman D, Asad H, Oliva E, et al. A limited panel of immunomarkers can reliably distinguish between clear cell and high-grade serous carcinoma of the ovary. *Am J Surg Pathol* 2009;**33**:14-21.
46. Xie A-Y, Bermudez VP, Folk WR. Stimulation of DNA replication from the polyomavirus origin by PCAF and GCN5 acetyltransferases: acetylation of large T antigen. *Mol Cell Biol* 2002;**22**:7907-18.
47. Surowiak P, Materna V, Maciejczyk A, Kaplenko I, Spaczynski M, Dietel M, et al. CD46 expression is indicative of shorter revival-free survival for ovarian cancer patients. *Anticancer Res* 2006;**26**:4943-8.
48. Maciejczyk A, Szelachowska J, Szynglarewicz B, Szulc R, Szulc A, Wysocka T, et al. CD46 expression is an unfavorable prognostic factor in breast Cancer cases. *Appl Immunohistochem Mol Morphol* 2011;**19**:540-6.
49. Dupont S. Role of YAP/TAZ in cell-matrix adhesion-mediated signalling and mechanotransduction. *Exp Cell Res* 2016;**343**:42-53.
50. Zhang C, Han Y, Huang H, Qu L, Shou C. High NR2F2 transcript level is associated with increased survival and its expression inhibits TGF-β-dependent epithelial-mesenchymal transition in breast cancer. *Breast Cancer Res Treat* 2014;**147**:265-81.
51. Parsons JT, Horwitz AR, Schwartz MA. Cell adhesion: integrating cytoskeletal dynamics and cellular tension. *Nat Rev Mol Cell Biol* 2010;**11**:633-43.
52. Rother J, Nöding H, Mey I, Janshoff A. Atomic force microscopy-based microrheology reveals significant differences in the viscoelastic response between malign and benign cell lines. *Open Biol* 2014;**4**:140046.